Materials Science-Poland, 33(4), 2015, pp. 751-759
http://www.materialsscience.pwr.wroc.pl/
DOI: 10.1515/msp-2015-0112

DE GRUYTER OPEN

Study of structural, morphological, optical and electroluminescent properties of undoped ZnO nanorods grown by a simple chemical precipitation

A. SINGH*, H.L. VISHWAKARMA

[1]Department of Physics, Rungta College of Engineering and Technology, Kohka Kurud Road, Bhilai (C.G.), India
[2]Department of Physics, Surguja University (C.G), India

In this work, zinc oxide (ZnO) nanorods were obtained by a simple chemical precipitation method in the presence of capping agent: polyvinyl pyrrolidone (PVP) at room temperature. X-ray diffraction (XRD) result indicates that the synthesized undoped ZnO nanorods have hexagonal wurtzite structure without any impurities. It has been observed that the growth direction of the prepared ZnO nanorods is [1 0 1]. XRD analysis revealed that the nanorods have the crystallite size of 49 nm. Crystallite size is calculated by Debye-Scherrer formula and lattice strain is calculated by Williomson-Hall equation. Cell volume, Lorentz factor, Lorentz polarization factor, bond length, texture coefficient, lattice constants and dislocation density have also been studied. We also compared the interplanar spacings and relative peak intensities with their standard values at different angles. The scanning electron microscope (SEM) images confirmed the size and shape of these nanorods. It has been found that the diameter of the nanorods ranges from 1.52 μm to 1.61 μm and the length is about 4.89 μm. It has also been observed that at room temperature ultraviolet visible (UV-Vis) absorption band is around 355 nm (blue shifted as compared to the bulk). The average particle size has also been calculated by mathematical model of effective mass approximation equation, using UV-Vis absorption peak. Finally, the bandgap has been calculated using UV-absorption peak. Electroluminescence (EL) studies show that emission of light is possible at very small threshold voltage and it increases rapidly with increasing applied voltage. It is seen that smaller ZnO nanoparticles give higher electroluminescence brightness starting at lower threshold voltage. The brightness is also affected by increasing the frequency of AC signal.

Keywords: *electroluminescence; optoelectronics; nanomaterials; nanorods; zinc oxide*

1. Introduction

In recent years one dimensional nanostructure materials, such as nanorods, nanowires and nanotubes have received much attention due to their remarkable properties. These properties are very useful in all fields, such as optoelectronics, electronic nanodevices, etc. [1, 2]. To understand the basic phenomena of quantum size effect on electrical, optical, mechanical and magnetic properties, some important semiconductor nanomaterials, such as GaN [3], CdS [4], Si [5], SnO_2 [6], TiO_2 [7], ZnO [8, 9] and CeO_2 [10–13] have been widely studied. Among them ZnO nanomaterials have been chosen because of their remarkable properties, like wide and direct bandgap ($E_g \sim 3.4$ eV) and large exciton binding energy (60 meV). UV lasing action is possible at room temperature due to wide bandgap and large exciton binding energy as explained by Park et al. [14]. In ZnO, due to the extremely large binding energy, the excitons are thermally stable. Due to all these reasons ZnO has significant advantages in optoelectronic applications, such as ultraviolet (UV) lasing media [15]. The wide and direct optical energy band gap of 3.37 eV is large enough to transmit most of the useful solar radiation for ZnO. ZnO is an n-type semiconductor belonging to II – VI group which is very useful for transparent electrodes in flat panel displays, solar cells and a promising material for short wavelength light emitting devices [16–18]. Its epitaxial films and

*E-mail: singh_nk24@yahoo.com

nanostructures have been mostly studied for the applications in UV-emitters, solar cells, gas sensors, varistors and surface electro-acoustic wave devices as given by Ozgur et al. [19]. Low dimensional nanostructures are now being extensively used in the field of advanced devices.

For electroluminescence devices, ZnO is one of the most widely investigated phosphor. Ahmed [20] found that the EL performance of alternating current devices is a strong function of crystallinity of the phosphor, its interface properties, space charge in the phosphor, the nature of the luminescent centers and their coordinates in the host crystal lattice.

For synthesis of nanomaterials there are various methods, such as chemical vapor deposition [21], laser ablation [22], vacuum arc deposition [23], sputtering [24] and hydrothermal process [25, 26]. But most of these fabrication techniques have complex steps, which require extremely sophisticated instruments, precise experimental setup and extreme experimental conditions. Hence, it is important to develop a very simple method to fabricate ZnO nanorods in laboratory environment. The chemical precipitation method provides a facile route to fabricate multidimensional nanostructures on a very large scale. This technique is inexpensive, and it does not require any complicated processing or huge infrastructure.

In this experiment, chemical precipitation method has been used for synthesis of hexagonal zinc oxide nanorods at room temperature, which is simple and economical. In this method zinc acetate and sodium hydroxide are used as precursors, polyvinyl pyrrolidone is used as a capping agent and deionised water as a solvent. Further, the samples have been characterized by XRD and SEM. Optical properties obtained by UV-Vis spectroscopy and electroluminescence of ZnO nanorods are also discussed.

2. Experimental

2.1. Materials

Zinc acetate dihydrate $Zn(CH_3COO)_2{\cdot}2H_2O$, sodium hydroxide (NaOH), polyvinyl pyrrolidone (PVP) and absolute ethanol were used to synthesize undoped zinc oxide nanorods. All these chemicals were used as precursors which were obtained from Merck Chemical Company. PVP was used as a capping agent. In this experiment, all the glassware used was acid washed. The chemical reagents used were analytical reagent grade which needs no further purification. Ultrapure water was used for all dilutions and sample preparation. The whole fabrication process was done at room temperature.

2.2. Sample preparation

In a typical experiment, 2.2 g (0.2 mol/L) of zinc acetate $Zn(CH_3COOH)_2{\cdot}2H_2O$ was dissolved in 50 mL deionized water. The stirring rate of the solution was 1200 rpm and the process was conducted at room temperature. Then 1g of PVP was dissolved in 50 mL deionized water and was added drop by drop to the constantly stirred solution for stabilizing the synthesized particles. The mixture was stirred at room temperature until a homogeneous solution was obtained. After that 0.4 g (0.2 mol/L) of 50 mL sodium hydroxide was added drop by drop to the above mixture which gave white voluminous precipitate. The stirring process was continued for 3 hours till the white precipitate deposited at the bottom of the beaker. This solution was kept overnight for settlement of precipitate. Then the precipitate was filtered and washed 2 or 3 times with distilled water and 1 or 2 times with absolute ethanol by using Whatmann filter paper. After this process the products were finally dried in a hot air oven at 100 °C for 1 hour. The powder obtained was used for further characterization process.

2.3. Characterization

The X-ray diffraction (XRD) patterns of the undoped powdered ZnO sample was recorded by X'Pert PRO diffractometer system using CuKα radiation ($\lambda = 1.54056$ Å) at 45 kV and 40 mA. The morphology and size of the particles were determined by scanning electron microscopy (SEM) using JEOL-EO microscope with an accelerating voltage of 20 kV. The optical absorption spectra of the particles were recorded using Perkin Elmer

Lambda-45 spectrophotometer in the wavelength range of 200 to 800 nm.

2.4. Formation of electroluminescence cell

The electroluminescence cell was prepared by using a triple layer structure. In this cell nanoparticle emission layer were sandwiched between two electrodes. The transparent electrode was prepared by depositing a thin film of indium tin oxide (ITO) on a clean glass substrate. This ITO coated glass behaved as an electrode. The surface resistivity of this electrode was 70 to 100 Ω/sq and L (length) × W (width) × T (thickness) was about 75 mm × 25 mm × 1.1 mm. Then, a mica sheet having a window of 2 × 2 mm was placed on a conducting glass plate so that the window was on the film of ZnO sample. An aluminium foil strip was placed tightly over this window so as to provide a good contact without an air gap with the ZnO nanoparticles film. The aluminium strip acted as a second electrode (area of 1 cm^2 and thickness of ∼100 Å). The layer of nanoparticles should be uniform and thin. Alternating voltage of various frequencies was applied and EL brightness (B) at different voltages (V) was measured with the help of a photomultiplier tube and corresponding current was also recorded.

3. Results and discussions

3.1. Structural studies

A typical XRD pattern of the prepared nanorods is shown in Fig. 1. The pattern obtained has been indexed as a hexagonal unit cell with wurtzite structure (JCPDS Card No. 36-1451). The observed relative peak intensities and interplanar spacing have been compared to that of their standard values which is given in Table 1. All peaks of the obtained product correspond to the hexagonal wurtzite structure of Zn which was studied by many researchers. In Fig. 1, the detected peaks are at 2θ values of 31.8384°, 34.4937°, 36.40840°, 47.57920° and 56.65420° corresponding to the lattice planes (1 0 0), (0 0 2), (1 0 1), (1 0 2) and (1 1 0), respectively. It has been observed that there is a small difference in the relative peak intensities of the lattice planes (1 0 0) to (0 0 2) and in the d-spacing of different peaks. It has also been observed that the XRD patterns of the nanorods are relatively broad because the crystals are randomly arranged or have low degree of periodicity. Furthermore, no impurities were found in the XRD pattern. This result shows that high purity hexagonal ZnO nanorods could be obtained by this chemical method.

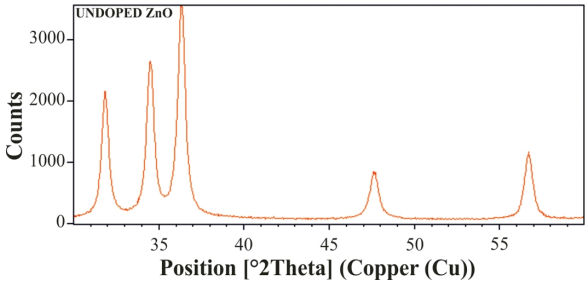

Fig. 1. XRD pattern of undoped ZnO nanorods.

The interplaner spacing (d), which is given in Table 1, has been evaluated using the relation 1 as explained by Mazhdi et al. [27]:

$$\frac{1}{d^2} = \frac{4}{3}\left(\frac{h^2+hk+k^2}{a^2}\right) + \frac{l^2}{c^2} \tag{1}$$

where a and c are the lattice constants defined as follows:

$$a = \frac{\lambda}{\sqrt{3}\sin\theta} \tag{2}$$

For (1 0 0) plane, the lattice constant a has been calculated by using equation 2 as explained by Cullity et al. [28] and found to be a = 3.2428 Å, while:

$$c = \frac{\lambda}{\sin\theta} \tag{3}$$

Similarly, for (0 0 2) plane, the lattice constant c has been calculated by using equation 3 as explained by Cullity et al. [28] and found to be c = 5.1960 Å.

Hence, the ratio c/a = 1.6023. Also, the diffraction peaks corresponding to the planes (1 0 0), (0 0 2), (1 0 1), (1 0 2) and (1 1 0) obtained from X-ray diffraction data are consistent with the

JCPDS data of ZnO. The interplanar spacing (d) calculated from XRD has been compared with JCPDS data card and corresponding (h k l) planes are summarized in Table 1.

The crystallite size (D) has been calculated by Debye-Scherrer formula using the raw data from XRD patterns. The formula is given in relation 4 and the calculated values are given in Table 2:

$$D = \frac{k\lambda}{\beta \cos\theta} \tag{4}$$

where k is a constant (0.9), D is the crystallite size (in nm), λ is wavelength (0.15406 nm), β is full width at half maximum (FWHM in radian) and θ is the Bragg diffraction angle [29].

Quantitative information concerning the preferential crystal orientation can be obtained from the texture coefficient (T_c), which is defined as in relation 5 given by Ilican et al. [30]:

$$T_c(hkl) = \frac{I(hkl)/I_o(hkl)}{\frac{1}{n}\sum_n I(hkl)/I_o(hkl)]} \tag{5}$$

where T_c (h k l) is the texture coefficient, I (h k l) is the XRD intensity, n is the number of diffraction peaks considered and I_o (h k l) is the standard intensity of the plane which is taken from JCPDS data as given in the literature [31, 32].

If T_c (h k l) ≈ 1 for all the considered (h k l) planes then the particles are randomly oriented crystallites which is similar to the JCPDS references. If the values of Tc(h k l) is greater than 1, it indicates that the abundance of grain is formed in a given [h k l] direction. If $0 < T_c$ (h k l) < 1 it indicates that there is a lack of grains in that given direction. As T_c (h k l) increases, the preferential growth of the crystallites in the direction perpendicular to the (h k l) plane is greater. This is shown in Table 1.

The relative percentage errors for all the particles which are shown in Table 1 have been evaluated by equation 6 and JCPDS standard d-values as given by Pathinettam et al. [33]:

$$\text{Relative percentage error} = \frac{Z_H - Z}{Z} \times 100\ \% \tag{6}$$

where Z_H is the obtained actual d-value in XRD pattern, Z is the standard d-value in JCPDS data. The values of 2θ, d-values, and d % error for the crystalline ZnO nanorods have been calculated by using equation 4 and are given in Table 1. The average relative percentage error is found to be 0.21 %, 0.11 %, 0.33 %, 0.003 % and 0.083 %, respectively. The experimental d-values and JCPDS d-values are approximately equal and suggest hexagonal structure [34].

The ZnO bond length L shown in Table 2 is given by equation 7 as explained by Yakuphanoglu et al. [35]:

$$L = \sqrt{\frac{a^2}{3} + \left(\frac{1}{2} - u\right)^2 c^2} \tag{7}$$

where u is the positional parameter in the wurtzite structure which is related to c/a ratio, u is a measure of the amount by which each atom is displaced with respect to the next, along the 'c' axis and is given by:

$$u = \frac{a^2}{3c^2} + 0.25 \tag{8}$$

The dislocation density (δ) as given by Williamson and Smallman's formula, shown in Table 3, represents the amount of defects in the powder which is determined by relation 9. The larger D and smaller FWHM values indicate better crystallization of the particles [36]:

$$\delta = \frac{1}{D^2} \tag{9}$$

The volume (V) of the hexagonal cell has been calculated by equation 10 and shown in Table 2 [37]:

$$V = \frac{\sqrt{3}}{2} a^2 c \tag{10}$$

The strain (ε) induced in the powders due to crystal imperfection and distortion has been calculated by Williamson-Hall method using equation 11 and line breadth ($\beta_{hkl} \cos\theta$), which is shown in Table 2, has been calculated by equation 12 [38]:

$$\varepsilon = \frac{\beta_{hkl}}{4 \tan\theta} \tag{11}$$

Table 1. Comparison of X-ray diffraction peak intensities, 2θ, d-values, and d % error of the JCPDS data in comparison with the observed data.

XRD peak (h k l)	2θ (degree) observed	2θ (degree) from JCPDS	Intensity observed	Intensity from JCPDS	d-spacing observed (Å)	d-spacing from JCPDS (Å)	Texture Coefficient T_c (h k l)	Relative percentage error
1 0 0	31.8384	31.770	61.64	57	2.80842	2.81430	1.11	0.21 %
0 0 2	34.4937	34.422	76.20	44	2.60022	2.60332	1.7	0.11 %
1 0 1	36.4084	36.253	100	100	2.46775	2.47592	1.03	0.33 %
1 0 2	47.5792	47.539	21	23	1.91120	1.91114	0.94	0.003 %
1 1 0	56.6542	56.603	30.60	32	1.62337	1.62472	0.98	0.083 %

Table 2. Volume, bond length, strain, line breadth, FWHM and particle size.

Volume V $(Å)^3$	Bond length L (Å)	Strain ε	Line breadth β h k l cosθ	FWHM β (degree)	Particle size D (nm)
51.151	2.0281	0.007273	0.009503	0.1020	91
40.496	1.8763	0.014281	0.020002	0.1840	45.23
34.618	1.7807	0.017882	0.025949	0.2175	38.47
16.080	1.3791	0.036876	0.064840	0.3346	25.96
9.879	1.2052	0.060482	0.121686	0.4488	20.12

$$\beta_{hkl}\cos\theta = \frac{k\lambda}{D} + 4\varepsilon\sin\theta \tag{12}$$

Integral breadth (β) of ZnO, which is given in Table 3, has been obtained from XRD patterns using relation 13 [39]:

$$\beta = \frac{Area}{I_o} \tag{13}$$

where Area = area under peak, I_o = maximum intensity.

The Lorentz-polarization factor is the most important of the experimental quantities that control X-ray intensity with respect to diffraction angle. In the intensity calculations, the Lorentz factor is combined with the polarization factor and further the variation of the Lorentz factor with the Bragg angle θ [40–42]. The overall effect of Lorentz factor is to decrease the intensity of the reflections at intermediate angles compared to those in the forward or backward directions. Lorentz factor and Lorentz polarization factor shown in Table 3 have been calculated from equation 14 and 15:

$$\text{Lorentz factor} = \frac{\cos\theta}{\sin^2 2\theta} = \frac{1}{4\sin^2\theta\cos\theta} \tag{14}$$

$$\text{Lorentz polarization factor} = \frac{1+\cos^2(2\theta)}{\sin^2\theta\cos\theta} \tag{15}$$

3.2. Morphological study

Fig. 2 presents the SEM image of ZnO nanorods at different magnifications. These pictures confirm the formation of ZnO nanorods. It is clear from Fig. 2a that the size of the nanorods is 10 μm. From the amplified SEM image it is clear that the ZnO nanorods are hexagonal in structure as shown in Fig. 2b, 2c and 2d. The powder contains ZnO nanorods of diameter 1.52 μm to 1.61 μm and length of 4.89 μm. In this work, the two main reactants used to fabricate ZnO were NaOH and $Zn(CH_3COO)_2{\cdot}2H_2O$. The solubility of these reactants in water (109 g/L and 30 g/L) is much higher than in other solvents. The high solubility is the main factor which decreases the number of nucleation sites [43].

3.3. Optical properties

UV-Vis absorption spectra of the ZnO nanorods are shown in Fig. 3. The optical properties are strongly dependent on the particle size. The room

Table 3. Dislocation density, integral breadth, Lorentz factor, Lorentz polarization factor.

Dislocation density (δ) $(nm)^{-2}$	Integral breadth (β)	Lorentz factor	Lorentz polarization factor
0.000120758	2.3772	3.4557	23.7987
0.000535093	4.5163	2.9778	20.0026
0.000675702	7.0045	2.6965	17.7724
0.001483852	2.3407	1.6791	9.7726
0.002470267	5.9797	1.2614	6.5701

temperature spectra exhibit strong excitonic absorption peak at 355 nm. The absorption spectrum shows a well-defined exciton band at 355 nm and a significant blue shift relative to the bulk exciton absorption (373 nm) [44]. This blue shift phenomenon is mainly related to the quantum confinement effect due to the small size of ZnO [45]. The most direct way of extracting the optical bandgap is to simply determine the photon energy at which there is a sudden increase in the absorption. For bulk samples, the bandgap is estimated from the $(\alpha h\nu)^2$ vs. $(h\nu)$ plot, where α is the absorption coefficient and $h\nu$ is the photon energy. But for nanocrystalline samples the bandgap is determined from absorption maxima. The optical bandgap E_g of the nanocrystalline samples is calculated from the absorption peak using the formula, $E_g = \hbar c/\lambda$, where $\hbar$ is Planck's constant, c is the velocity of light and λ is the wavelength of the light at which absorption peak is obtained. The bandgap of ZnO has been found to be 3.4 eV.

The average particle size in a nanocolloid can be calculated from the absorption onset of UV-Vis absorption spectra (Fig. 3) by using effective mass model [46, 47], where the bandgap E* can be approximated by:

$$E^* = E_g^{bulk} + \frac{\hbar^2\pi^2}{2er^2}\left(\frac{1}{m_e^* m_0} + \frac{1}{m_h^* m_0}\right) - \frac{1.8e}{4\pi\varepsilon\varepsilon_0 r} - \frac{0.124e^3}{\hbar^2(4\pi\varepsilon\varepsilon_0)^2}\left(\frac{1}{m_e^* m_0} + \frac{1}{m_h^* m_0}\right)^{-1} \quad (16)$$

where E_g^{bulk} is the bulk bandgap expressed in eV, $\hbar$ is Planck's constant, r is a particle radius, m_e is the electron effective mass, m_h is the hole effective mass, m_0 is free electron mass, e is the electron charge, ε is the relative permittivity and ε_0 is the permittivity of free space. Due to the relatively small effective masses of ZnO ($m_e = 0.26$, $m_h = 0.59$) the bandgap enlargement is expected for the particle having radii less than about 4 nm [45, 46]. The following equation has been derived from the effective mass model given above with small mathematical simplification [48] which has been used to find the size of the particle from the absorbance spectra.

The average particle size of the nanoparticles can be determined by using the mathematical model of the effective mass approximation equation 17 as explained in the literature [48, 49]:

$$r(nm) = \frac{-0.3049 + \sqrt{-26.23012 + \frac{10240.72}{\lambda_p(nm)}}}{-6.3829 + \frac{2483.2}{\lambda_p(nm)}} \quad (17)$$

where r is radius of the particle, λp is the peak absorbance wavelength for monodispersed ZnO nanoparticles, $m_e = 0.26\ m_o$, $m_h = 0.59\ m_o$, m_o is the free electron mass, $\varepsilon = 8.5$ and $E_g^{bulk} = 3.3$ eV. The prepared ZnO nanorods show the absorbance peak at 355 nm which corresponds to average particle size of 2.15 nm.

3.4. Electroluminescence studies

The voltage brightness characteristics for undoped ZnO nanorods are shown in Fig. 4. EL studies of undoped ZnO nanorods show that light emission occurs at a certain threshold voltage and then increases rapidly with an increase in voltage. It is noted that at lower voltages the increase in brightness is comparatively slow, but becomes quite fast at higher voltages. The threshold voltage and maximum EL brightness depend on the value

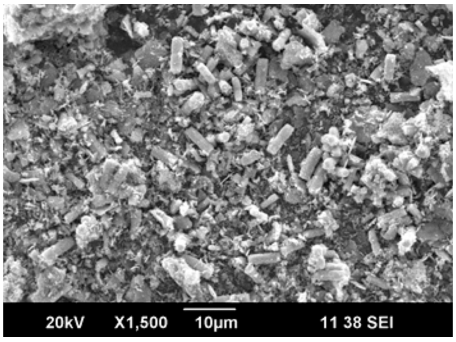

(a)

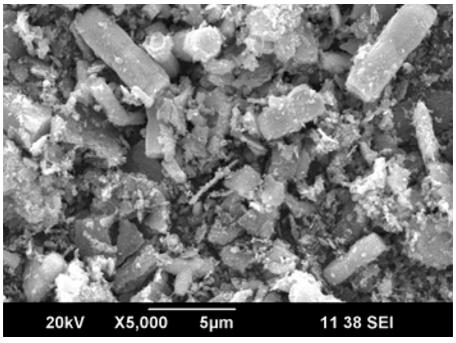

(b)

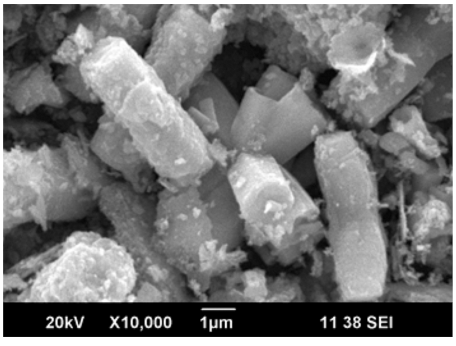

(c)

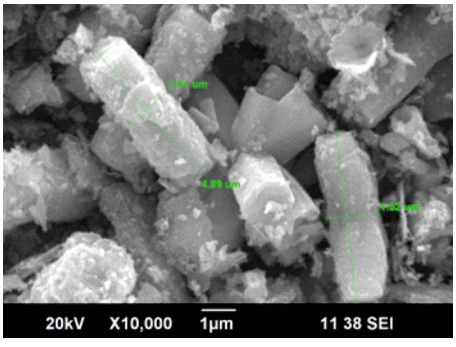

(d)

Fig. 2. SEM images of undoped ZnO nanorods at (a) low, (b) high, (c) and (d) very high magnification ((d) includes nanorods dimensions).

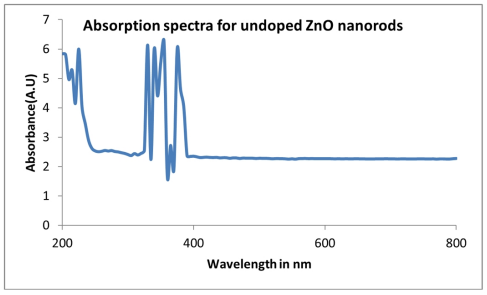

Fig. 3. UV-Vis absorption spectrum of undoped ZnO nanorods.

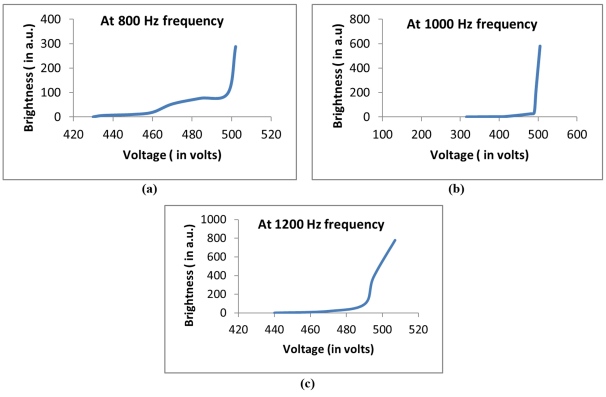

Fig. 4. Voltage-brightness characteristics of undoped ZnO nanorods at frequencies of (a) 800 Hz, (b) 1000 Hz, (c) 1200 Hz.

of AC frequency. The reason of higher EL brightness is that when the voltage increases, more electrons and holes are injected into the emission layer. Due to recombination, the brightness is increased with increasing voltage. At high applied voltages, electrons tunnel from the interface states into conduction band of the active layer. At a high electric field, electrons accelerate and it excites the activator ions. As a result, the threshold voltage is related primarily to electrons tunneling which is induced by electric field. The EL brightness behavior with variation of voltage is in agreement with excitation-collision mechanism and formation of Mott-Schottky barrier.

I-V characteristics of ZnO nanorods at different frequencies are shown in Fig. 5. It is found that upon increasing frequency of an input AC signal, EL brightness increases continuously. This indicates an ohmic contact between the sample and

the electrodes. The relation between the current and voltage is found to be linear in the frequency range of 800 to 1200 Hz.

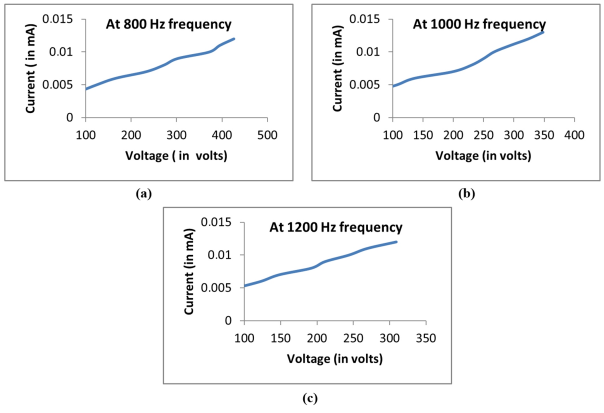

Fig. 5. Voltage-current curve for undoped ZnO nanorods at frequencies of (a) 800 Hz, (b) 1000 Hz, (c) 1200 Hz.

4. Conclusions

ZnO nanorods with diameters of 1.52 to 1.61 μm and length of 4.89 μm have been successfully prepared by a simple chemical precipitation method at room temperature. In the sample preparation zinc acetate dihydrate was used as a precursor and polyvinyl pyrrolidone was used as a capping agent. The XRD patterns obtained confirmed the formation of wurtzite hexagonal ZnO nanostructures without any impurities. The XRD studies of these nanorods revealed that their average size, which was calculated by Debye-Scherrer formula, is about 49 nm for undoped ZnO. Also, d-spacing and relative peak intensities have been compared with their standard values. Relative intensity for the lattice plane (1 0 1) and d-spacing for the lattice planes (1 0 2) and (1 1 0) were found nearly equal. The highest texture coefficient was found for (1 0 1) plane for undoped ZnO. The bond length of 1.7151 Å is consistent with ZnO unit cell. The size and strain contribution has been analyzed by the method of Williamson and Hall. Further, the UV absorption at ∼355 nm was found blue shifted; energy band gap of ZnO was calculated as 3.4 eV. From UV-Vis absorption spectra, the calculated average size of prepared undoped ZnO nanorods was found to be 2.44 nm from peak absorption wavelength. Hence, it is concluded that in the presence of deionized water as a solvent, the size of ZnO nanorods is in micro range. EL studies have shown that the light emission starts from undoped ZnO nanorods at lower threshold voltage and higher EL intensity is obtained in case of smaller particles. Thus, high efficiency EL devices for display and lightening can be fabricated by using small size undoped ZnO nanorods. This study provides a new approach to change the optical properties, which can be used for further optoelectronic applications.

Acknowledgements

The authors are thankful to the SAIF Kochi, Ernakulum, for characterization of samples by SEM technique, the SAIF Panjab University, Chandigarh, for XRD studies and the CIL Panjab University for UV-Vis absorption spectra of the given samples. We are also thankful to Dr. M. Ramrakhyani for giving us opportunity to perform electroluminescent study in the RDVV University.

References

[1] Morales A.M., Lieber C.M., *Science*, 279 (1998), 208.
[2] Dai H., Wong E.W., Lu Y.Z., Shoushan F., Lieber C.M., *Nature*, 375 (1995), 769.
[3] Han W.Q., Fan S.S., Li Q.Q., Hu Y.D., *Science*, 277 (1997), 1287.
[4] Zhan J.H., Yang X.G., Wang D.W., Li S.D., Xie Y., Xia Y.N., Qian Y.T., *Adv. Mater.*, 12 (2000), 1348.
[5] Hu J., Odom T.W., Lieber C.M., *Accounts Chem. Res.*, 5 (1999), 435.
[6] Rai R., *Adv. Mater. Lett.*, 1 (2010), 55.
[7] Chen L., Pang X., Guangshui Y., Zhang J., *Adv. Mater. Lett.*, 1 (2010), 75.
[8] Gautam S., Kumar S., Thakur P., Chae K.H., Kumar R., Koo B.H., Lee C.G., *J. Phys. D Appl. Phys.*, 42 (2009), 175406.
[9] Azam A., Ahmed F., Arshi N., Chaman M., Naqvi A.H., *J. Alloy. Compd.*, 496 (2010), 399.
[10] Kumar S., Kim G.W., Koo B.H., Sharma S.K., Knobel M., Chung H., Lee C.G., *J. Nanosci. Nanotechno.*, 11 (2011), 555.
[11] Kumar S., Kim Y.J., Koo B.H., Lee C.G., *J. Nanosci. Nanotechno.*, 10 (2010), 7204.
[12] Kumar S., Kim Y.J., Koo B.H., Choi H.K., Lee C.G., *IEEE T. Magn.*, 45 (2009), 2439.
[13] Kumar S., Kim Y.J., Koo B.H., Sharma S.K., Knobel M., Meneses C.T., Shukla D.K., Kumar R., Lee C.G., *J. Korean Phys. Soc.*, 55 (2009), 10108.
[14] Park Y.K., Inhan J., Kwak M.G., Yang H., Ju S.H., Cho W.S., *J. Lumin.*, 78 (1998), 87.

[15] ZHAO Q.X., WILLANDER M., MORJAN R.E., HU Q.H., CAMPBELL E.E.B., *Appl. Phys. Lett.*, 83 (2003), 165.
[16] ELMER K., *J. Phys. D Appl. Phys*, 33 (2000), 17.
[17] KRUNKS M., MELLIKOV E., *Thin Solid Films*, 270 (1995), 33.
[18] ARANOVICH J.A., GOLMAYO D., FAHRENBRUCH A.L., BUBE R.H., *J. Appl. Phys.*, 51 (1980), 4260.
[19] OZGUR U., ALIVOV Y.I., LIU C., TEKE A., RESHCHIKOV M.A., DOGAN S., AVRUTIN V., CHO S.J., MORKOC H., *J. Appl. Phys.*, 98 (2005), 04130.
[20] AHMED M.A.A., *Phosphor materials and luminescent impurities for ACTFEL device*, Brno University of Technology, Brno, 2004, p. 8.
[21] JIH-JEN W., SAI-CHANG L., *Adv. Mater.*, 14 (2002), 215.
[22] FOUCHET A., PRELLIER W., MERCEY B., MECHIN L., KULKARNI V.N., VENKTESAN T., *J. Appl. Phys.*, 96 (2004), 3228.
[23] TAKIKAWA H., KIMURA K., MIYANO R., SAKAKIBARA T., *Thin Solid Films*, 377 (2000), 74.
[24] WANG Q.P., ZHANG D.H., XUE Z.Y., HAO X.T., *Appl. Surf. Sci.*, 201 (2002), 123.
[25] HANMEI H., *Mater. Chem. Phys.*, 106 (2007), 58.
[26] EFTEKHARI A., MOLAEI F., ARAMI H., *Mat. Sci. Eng. A-Struct.*, 437 (2006), 446.
[27] MAZHDI M., HOSSEIN KHANI P., *Int. J. Nano Dimens.*, 4 (2012), 233.
[28] CULLITY B.D., STOCK S.R., *Elements of X-ray diffraction*, Prentice Hall, New Jersey, 2001.
[29] KHORSAND ZAK A., MAJID ABD W.H., ABRISHAMI M.E., YOUSEFI R., *Solid State Sci.*, 13 (2011), 251.
[30] ILICAN S., CAGLAR Y., CAGLAR M., *J. Optoelectron. Adv. M.*, 10 (2008), 2578.
[31] JOINT COMMITTEE ON POWDER DIFFRACTION STANDARDS, *Powder Diffraction File*, Card No.: 89-1397.
[32] SCHULZ H., THIEMANN K.H., *Solid State Commun.*, 9 (1979), 783.
[33] PATHINETTAM P.D., MARIKANI A., *Cryst. Res. Technol.*, 11 (2002), 1241.
[34] JOINT COMMITTEE ON POWDER DIFFRACTION STANDARDS, *Powder Diffraction File*, Card No.: 36-1451.
[35] YAKUPHANOGLU F., ILICAN S., CAGLAR M., CAGLAR Y., *J. Optoelectron. Adv. M.*, 9 (2007), 2180.
[36] WILLIAMSON G.B., SMALLMAN R.C., *Philos. Mag.*, 1 (1956), 34.
[37] KITTEL C., *Introduction to Solid State Physics*, John Wiley & Sons, New York, 2005.
[38] YOGAMALAR R., SRINIVASAN R., VINU A., ARIGA K., BOSE A.C., *Solid State Commun.*, 149 (2009), 1919.
[39] SUTTA P., JACKULIAK Q., *Mater. Struct.*, 5 (1998), 10.
[40] PEISER H.S., ROOKSBY H.P., WILSON A.J.C., *X-ray Diffraction by Polycrystalline Materials*, Institute of Physics, London, 1955.
[41] CLARK G.L., *Applied X-rays*, McGraw- Hill Book Company, New York, 1955.
[42] COMPTON A.H., ALLISON S.K., *X-rays in Theory and Experiment*, D. Van Nostrand Company, New York, 1935.
[43] ZHAO J., YAN X., LEI Y., ZHAO Y., HUANG Y., ZHANG Y., *Adv. Mater. Res.*, 1 (2012), 75.
[44] HAASE M., WELLER H., HENGLEIN A., *J. Phys. Chem.*, 92 (1988), 482.
[45] KOCH U., FOJTIK A., WELLER H., HENGLEIN A., *Chem. Phys. Lett.*, 122 (1985), 507.
[46] SHIONOYA S., YEN W.M., YAMAMOTO H., *Phosphor Handbook*, CRC Press, USA, 1998.
[47] BERGER L.I., *Semiconductor Materials*, CRC Press, USA, 1997.
[48] BRUS L., *J. Phys. Chem. A*, 12 (1986), 2555.
[49] PESIKA N.S., STEBE K.J., SEARSON P.C., *Adv. Mater.*, 15 (2003), 1289.

Received 2014-12-09
Accepted 2015-09-22